

# Interplay of Surface Energy and Bulk Thermodynamic Forces in Ordered Block Copolymer Droplets

Su-Mi Hur,<sup>†,‡,⊥</sup> M. Serdar Onses,<sup>§,||</sup> Abelardo Ramírez-Hernández,<sup>†,‡</sup> Paul F. Nealey,<sup>‡,†</sup> John A. Rogers,<sup>\*,§</sup> and Juan J. de Pablo<sup>\*,‡,†</sup>

<sup>†</sup>Materials Science Division, Argonne National Laboratory, 9700 South Cass Avenue, Argonne, Illinois 60439, United States

<sup>‡</sup>Institute for Molecular Engineering, The University of Chicago, Chicago, Illinois 60637, United States

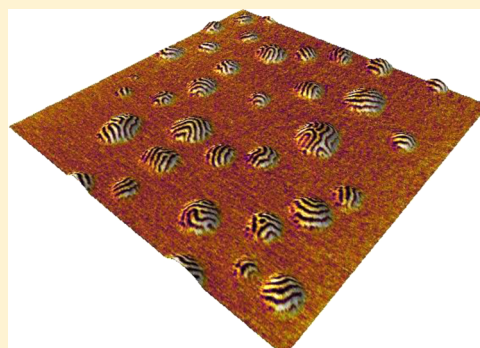
<sup>§</sup>Department of Materials Science and Engineering, Beckman Institute, and Frederick Seitz Materials Research Laboratory, University of Illinois at Urbana–Champaign, Urbana, Illinois 61801, United States

<sup>||</sup>Department of Materials Science and Engineering, Nanotechnology Research Center (ERNAM), Erciyes University, Kayseri 38039, Turkey

<sup>⊥</sup>School of Polymer Science and Engineering, Chonnam National University, Gwangju, 500-757, Korea

## Supporting Information

**ABSTRACT:** The wetting state of a simple liquid on a solid substrate, as summarized by Young's equation, is dictated by the interfacial energies of the different phases that coexist in the system. For simple fluids, rotational symmetry gives rise to symmetric droplets around the axis perpendicular to the substrate. This is not the case for nanostructured fluids, such as block copolymers, where the inherent thermodynamic ordering forces compete with surface tension. This competition is particularly important in nanoscale droplets, where the size of the droplets is a small multiple of the natural periodicity of the block copolymer in the bulk. In the nanoscale regime, droplet shape and internal structure arise from a subtle interplay between interfacial and bulk contributions to the free energy. In this work, we examine the consequences of surface–polymer interaction energies on droplet morphology through a concerted simulation and experimental effort. When the block copolymer is deposited on a neutral substrate, we find noncircular arrangements with perpendicular domains. However, when a preferential substrate is used, the resulting morphology depends on droplet size. In large droplets, we observe bottle-cap-shaped structures with a ring of perpendicular domains along the perimeter, while small droplets exhibit stripes of perpendicular domains.



## INTRODUCTION

The Young equation provides a simple relation between the equilibrium contact angle of a liquid droplet on a solid surface and the three interfacial tensions involved. If the three tensions are known, then the wetting state can be predicted directly.<sup>1</sup> When the fluid is a simple liquid, the shape of the droplet inherits the rotational symmetry of the fluid in the bulk. The situation is more complicated when the fluid of interest is an inherently structured liquid, such as a liquid crystal or a block copolymer (BCP), because rotational symmetry is broken due to the creation of domains arranged in lattices having a lower symmetry. In the particular case of block copolymers (BCPs), the self-assembled structures that are typically observed have characteristic dimensions that range from 5 to 100 nm.<sup>2,3</sup> The dimensions and symmetry of the structures depend on the number of blocks, composition, and architecture of the block copolymer.<sup>3,4</sup> In the bulk, the self-assembly is thermodynamically governed by an interplay between two competing weak forces: (i) the incompatibility between the blocks, which favors large domains and minimizes contacts between dissimilar

blocks, and (ii) the entropic force associated with chain elasticity. Under confinement, for example thin films, interfacial and bulk contributions to the total free energy have comparable magnitudes, and the subtle interplay between them leads to morphologies that are considerably different from those observed in the bulk.<sup>5</sup> The situation is even richer in block copolymer droplets, where one can engineer the wetting of the substrate to be different for distinct blocks. Moreover, blocks can exhibit a different surface energy, turning the free interface into a critical boundary condition.

Previous studies have explored the wetting behavior of large BCP droplets deposited on a solid substrate. In particular, by adopting a strong segregation approximation and pursuing experiments on the stability of parallel layers of BCP domains, Ausserre et al.<sup>36</sup> found that only mono- and bilayers (parallel lamellae) are stable when the spreading parameter is positive.

Received: March 25, 2015

Revised: June 11, 2015

Published: June 29, 2015

When the BCP is not wetting, the polymer domains are subjected to a “piling-up instability”, which leads to the formation of terraced structures, or so-called Babel towers. The latter consist of stacks of concentric circular disks of parallel lamellae. Limary et al.<sup>33,34</sup> and Knoll et al.<sup>38</sup> have discussed the critical role of the interplay between surface energies, ordering, and confinement on the self-assembly of polymer domains, for both lamellae- and cylinder-forming block copolymer thin films. More recently, Croll et al.<sup>37</sup> investigated how a BCP droplet shape is modified as the melt goes from the disordered to the lamellar phase. The droplets explored in that work had diameters larger than 6  $\mu\text{m}$  and heights around 200 nm. A strongly preferential substrate was used and the annealing temperature was such that asymmetric conditions were imposed on the droplets' interfaces. A transition from a smooth spherical cap to a terraced hyperbolic profile was found as the fluid went from the isotropic liquid to a structured material.<sup>37</sup> By using a nanoimprint lithography technique, Farrell et al.<sup>39</sup> were able to spatially control the dewetting process. By manipulating the geometry and chemistry of the templates, it was possible to generate uniform arrays of microsized droplets of microphase-separated BCP. These authors considered large droplets of cylinder-forming PS–PMMA copolymer ( $\approx 0.5$ – $1 \mu\text{m}$  in diameter), consisting of hexagonally closed-packed cylinders oriented perpendicular to the substrate. Small droplets ( $\approx 200$ – $300 \text{ nm}$  in diameter), however, led to the formation of parallel cylinders arranged in closed loops.<sup>39</sup>

In this work we present a systematic study of diblock copolymer morphology in small droplets. We present experimental data for polystyrene-*block*-poly(methyl methacrylate) (PS-*b*-PMMA) on different substrates. Experimental top-down micrographs and AFM measurements are then interpreted by resorting to a coarse-grained model of block copolymers that is able to predict the shape and three-dimensional morphology of copolymer droplets as a function of size and interaction with the substrate.

## MODELS AND METHODS

**Experiments. Preparation of Substrates.** Silicon wafers ( $\langle 100 \rangle$ , WRS Materials) were cleaned in a piranha solution ( $\text{H}_2\text{SO}_4:\text{H}_2\text{O}_2 = 7:3$ ) at  $130 \text{ }^\circ\text{C}$  for 30 min and then rinsed with water for three times 5 min each and then dried with  $\text{N}_2$ . A 0.2 wt % solution (toluene) of cross-linkable random copolymer was spin-cast onto the clean silicon wafers and cross-linked at  $250 \text{ }^\circ\text{C}$  for 5 min in a glovebox filled with  $\text{N}_2$ . Random copolymers were synthesized following the procedures reported in the previous study.<sup>6</sup> Random copolymers contained 4% glycidyl methacrylate with styrene and methyl methacrylate contents of 96%:0% and 57%:39%.

**Electrohydrodynamic Jet Printing.** Prepulled glass pipets (World Precision Instruments) with a tip inner diameter of  $1 \mu\text{m}$  were sputter-coated (Denton, Desk II TSC) with Au/Pd. Metal-coated nozzles were treated with a hydrophobic solution (0.1% perfluorodecanethiol in DMF) prior to printing for 10 min and then dipped in DMF for 10 s and dried with air to minimize the wetting of the nozzle with the ink. A 0.1% solution of PS-*b*-PMMA (37–37 kg/mol, Polymer Source Inc.) in 1,2,4-trichlorobenzene (99%, Sigma-Aldrich) served as the ink. A voltage (300–450 V) was applied between a metal-coated glass capillary and a grounded substrate with a standoff height of  $\sim 30 \mu\text{m}$ . Spatial control of the printing process was provided by a 5-axis stage interfaced to a computer that allowed coordinated control of voltage applied to the nozzle.<sup>7</sup> The voltage was typically chosen as slightly higher than the minimum voltage to initiate printing of fibrous structures.

**Generation and Characterization of BCP Droplets.** The substrates with printed fibrous BCP structures were annealed in a glovebox filled

with  $\text{N}_2$  or in a vacuum chamber at  $220 \text{ }^\circ\text{C}$  for different times that range from 5 min to 24 h, leading to formation of BCP droplets. The dimensions of the droplets depend on the structure of the printed features. In the conventional cone-jet mode, where continuous linear structures are printed, thermal annealing did not lead to BCP droplets (Supporting Information Figure S1). However, depending on the composition of the ink, a slight decrease in the voltage bias between the nozzle and the substrate could lead to printing of randomly oriented fibrous structures, which then transformed into BCP droplets during the thermal annealing step (i.e.,  $220 \text{ }^\circ\text{C}$  for 5 min). Here the dimensions of the droplets could be indirectly controlled by the printing conditions, including the applied voltage bias and stage speed. Lowering the voltage resulted in BCP droplets with smaller dimensions (Figure S1). Note, however, that the voltage window has a lower bound below which there was no material ejection from the nozzle. Additionally, printing at high stage speeds allowed access to smaller droplets by decreasing the overlap between the fibrous structures (Figure S2). The surface morphologies of the printed BCP films were imaged with a field emission SEM (Hitachi S-4800) at 1 kV. The topography of the films was analyzed with an AFM (Asylum Research MFP-3D) in tapping mode using a silicon tip with aluminum reflex coating (Budget Sensors). A plausible explanation for why the linear (and wider) BCP stripes did not lead to droplets could be that the annealing time was not sufficiently long to induce such a process; in other words, kinetic effects could come into play. Experiments and numerical studies of the breaking of thin fluid stripes on solid substrates have found that thinner lines break faster than thicker and wider ones. In the latter case, an end-driven instability plays a dominant role. To analyze such cases, a framework was developed to study a modified Plateau–Rayleigh instability that takes into consideration the presence of the solid surface (by including a disjoining pressure or van der Waals contribution).<sup>30–32</sup>

**Simulations.** The coarse-grained model adopted here relies on a molecular representation of the polymer.<sup>8</sup> Intermolecular interactions, however, are represented by functionals of the local densities of the different chemical species.<sup>9</sup> The model is defined by a set of parameters that can be mapped one-to-one with the experimental systems considered here and has been successful in past studies of the behavior of block copolymer films of uniform thickness.<sup>10</sup> Under “soft” confinement, as in a droplet, the confining surface can adapt to changes in the structure of the block copolymer melt, giving rise to a phase behavior that is much richer than that observed in uniform or “infinite” films. Consistent with past self-consistent field theory (SCFT) studies of polymeric materials at free interfaces,<sup>11–13</sup> we represent the air by a structureless fluid that creates an interfacial tension with the polymer melt. In our approach, copolymers are modeled as flexible linear chains described by the discretized Gaussian chain model, where the position of the  $t$ th bead in the  $i$ th chain is denoted by  $\mathbf{r}_i(t)$ . The air region is filled with an incompatible molecular fluid. The system is confined in a volume  $V$  at temperature  $T$ , and it is composed of  $n_{\text{AB}}$  diblock copolymer molecules and  $n_{\text{C}}$  structureless fluid particles. Each AB diblock copolymer consists of  $N_{\text{AB}}$  beads. Intramolecular interactions acting along the chains are given by

$$\frac{\mathcal{H}_b}{k_{\text{B}}T} = \frac{3}{2} \sum_{i=1}^{n_{\text{AB}}} \sum_{t=1}^{N_{\text{AB}}-1} \frac{[\mathbf{r}_i(t+1) - \mathbf{r}_i(t)]^2}{b^2} \quad (1)$$

where  $N_{\text{AB}}$  is the polymerization index of the block copolymer molecules and  $b^2$  is the mean-squared bond length of an ideal chain. The variable  $n = n_{\text{AB}} + n_{\text{C}}$  is used to denote the total number of molecules. Intermolecular interactions are given by<sup>8</sup>

$$\frac{\mathcal{H}_{\text{nb}}}{k_{\text{B}}T} = \rho_0 \int_V d\mathbf{r} \left[ \chi_{\text{AB}} \phi_{\text{A}} \phi_{\text{B}} + \chi_{\text{AC}} \phi_{\text{A}} \phi_{\text{C}} + \chi_{\text{BC}} \phi_{\text{B}} \phi_{\text{C}} + \frac{\kappa}{2} (\phi_{\text{A}} + \phi_{\text{B}} + \phi_{\text{C}} - 1)^2 \right] \quad (2)$$

where  $\phi_{\mu}(\mathbf{r})$  is the local dimensionless density of beads of type  $\mu$  ( $= \text{A, B, C}$ ) and  $\rho_0$  is the bead number density. The repulsion between

unlike monomers is represented by the first three terms in eq 2, where the Flory–Huggins parameters  $\chi_{\mu\nu}$  are used to quantify the strength of the corresponding interactions. The last term in eq 2 is the Helfand’s quadratic approximation,<sup>14</sup> which assigns a finite compressibility to the melt. The parameter  $\kappa$  is related to the inverse isothermal compressibility.<sup>15</sup>

The affinity of the substrate is described by a one-body potential acting on each bead and depends explicitly on the position and type of the bead. Thus, a potential of the form  $V = \sum_j U(\mathbf{r}_j, \mu_j)$  is added to the Hamiltonian of eq 2, where the sum runs over all beads and  $\mu_j$  denotes the type of the particle  $j$ . Following previous studies, the potential adopted here is of the form<sup>16</sup>

$$\frac{U(\mathbf{r}, \mu)}{k_B T} = -\frac{\lambda^\mu(x, y)}{\xi/R_c} e^{-z^2/2\xi^2} \quad (3)$$

This function decays over a short distance  $\xi$ .  $\lambda^\mu$  determines the strength of the interaction between the beads of type  $\mu$  and the substrate. The variable  $z$  represents the distance to the surface.

The equilibrium behavior of this model is explored by Monte Carlo simulations.<sup>17</sup> The local densities are defined on a lattice with a spacing  $\Delta L$  and computed from the beads’ positions by a particle-to-mesh interpolation (PM0).<sup>8</sup> The configurations are sampled according to Metropolis criteria,  $P_{acc} = \min[1, \exp(-\beta\Delta\mathcal{H})]$ , where  $\Delta\mathcal{H}$  is the energy change between two configurations. It includes both intra- and intermolecular contributions as well as any change of the one-body potential energy associated with the substrate. The trial moves considered here include reptation-like displacements, local displacements of the beads, and translations of an entire chain.<sup>8</sup>

The parameters that define the melt have the following values:  $\kappa N_{AB} = 35$ ,  $\chi_{AB} N_{AB} = 25$ , and  $\sqrt{N} = \rho_0 R_c^3 / N_{AB} = 110$ . Block copolymer chains are discretized into  $N_{AB} = 32$  beads; their bulk end-to-end distance  $R_c$  is set as the reference length scale. The bond length is fixed at  $b^2 = R_c^2 / (N_{AB} - 1)$ . The computed natural period of the lamellae in the bulk is  $L_0 = 1.66R_c$ . This parametrization corresponds to a PS-*b*-PMMA block copolymer with molecular weight MW = 74 kg/mol. Following the literature, the spacing of the lattice is chosen such that each bead interacts on average with  $n_{int} = 14$  particles.<sup>8</sup> For the interaction potential that describes the substrate we use  $\xi = 0.15R_c$ . The simulation box has large lateral dimensions to avoid finite size effects, and periodic boundary conditions are applied in all lateral directions. Note that for simplicity we have assumed that both blocks have the same surface energy (i.e.,  $\chi_{AC} = \chi_{BC} = 10\chi_{AB}$ ) and that the structureless fluid interacts with the substrate via a hard-wall interaction. At this point it is instructive to point out that multiple studies have shown that assembly of PS–PMMA diblocks leads to formation of islands and holes in films of incommensurate thickness with PS at the free surface. These observations indicate that PS has a lower surface energy than PMMA in the range of temperatures considered in such experiments. However, it has been shown that the segregation of PS at the free surface can be suppressed at temperatures larger than 230 °C.<sup>40–42</sup> These experimental results lead us to assume that for the annealing temperature considered in our work (220 °C) the difference in surface energy,  $\Delta\gamma$ , is small. Also note that for the case of nonpreferential (or patterned) substrates a small range of surface energy differences exists where one can obtain perpendicularly oriented lamellae.<sup>21–24</sup>

## RESULTS AND DISCUSSION

Diblock copolymers can adopt two wetting configurations: one in which polymer domains are oriented parallel to the substrate and another where domains are oriented perpendicular to it. In thin films, one can select one or the other configuration by controlling surface chemistry and film thickness. As alluded to earlier, by increasing the confinement’s dimensionality from 2D (infinite thin films) to 3D (droplets), new factors come into play and can alter the expected configurations. We deposited diblock copolymer droplets on two substrates: (i) one substrate

was covered by a PS-*r*-PMMA random copolymer mat with 56% PS content, which results in a nonpreferential substrate, and (ii) one substrate was covered by a PS-*r*-PMMA mat with 76% PS content, which is preferential to PS. As expected, block copolymer morphologies in the droplets depend not only on substrate composition but also on droplets size. As can be seen in Figure 1, on nonpreferential substrates droplets always

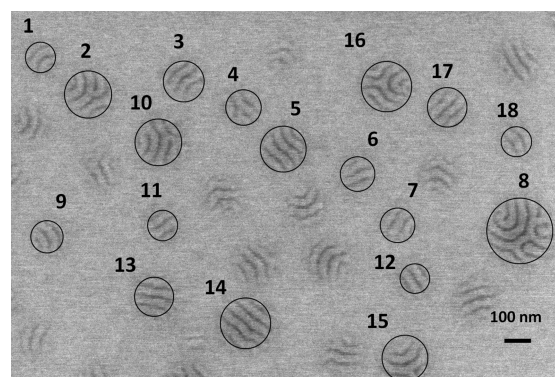


**Figure 1.** SEM image of self-assembled PS-*b*-PMMA nanodroplets formed on a nonpreferential substrate.

exhibit perpendicular domains, regardless of droplet size. As droplet size increases, the number of lamellae and that of internal domains also increases; these changes can be appreciated when comparing the droplet labeled as “1” in Figure 1 with those labeled as “3” and “5”. Eventually, large droplets start to exhibit multiple defects, as can be seen, for example, in the droplet labeled as “8”. Note that some droplets in the figure have been circled to highlight particular domain arrangements; the circles, however, are not meant to indicate that the droplet shape is circular. A detailed look at the SEM images reveals that some droplets adopt anisotropic shapes, although the boundary is not very well-defined. Further insights can be gained by combining phase and topography information obtained from AFM measurements. As can be seen in Figure 2, indeed some droplets display anisotropic shapes, whereas the height profiles for the more circular ones correspond to almost spherical caps.

A more interesting behavior arises when copolymer droplets are deposited on the PS-preferential substrate. In this case, simple intuition would suggest that a typical morphology should consist of parallel layers of PS and PMMA. However, as

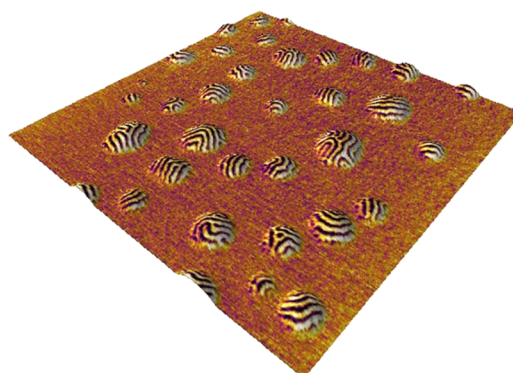


**Figure 2.** 3D topography image of the droplets colored with phase data of self-assembled PS-*b*-PMMA nanodroplets formed on a nonpreferential substrate.

can be seen in Figure 3, our experiments show a peculiar behavior in which morphology appears to depend on size.

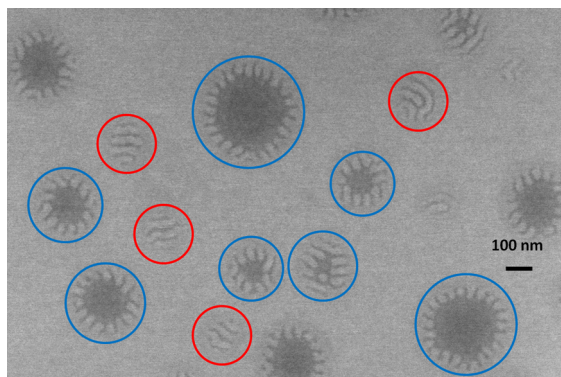


**Figure 3.** SEM image of self-assembled PS-*b*-PMMA nanodroplets formed on a PS-preferential substrate. The blue circles are used to highlight bottle-cap morphologies, and the red circles are used to highlight perpendicular morphologies.

Small droplets tend to display perpendicularly oriented copolymer domains. Beyond a certain droplet size, however, droplets adopt a “bottle cap” appearance, in which a ring of perpendicular domains is observed along the perimeter. We have quantified this phenomenon by measuring both the height profile and diameter of the droplets. We have classified the droplets’ structure into two categories: (1) perpendicular domains and (2) parallel lamellae with a ring of perpendicular domains. The results shown in Figure 4 show that there is a

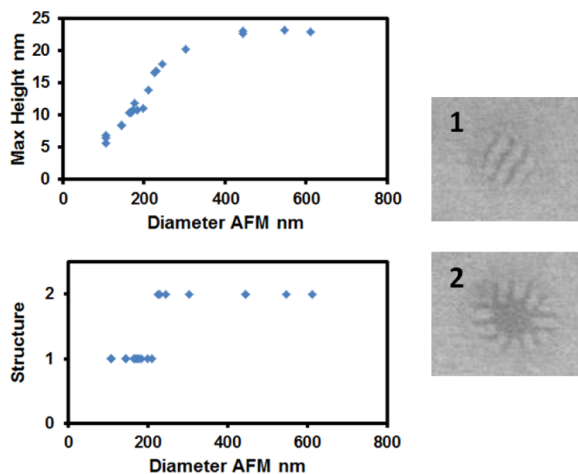


**Figure 4.** Correlation between droplet height, diameter, and morphology for block copolymers deposited on PS-preferential substrate. The images shown on the right, labeled as “1” and “2”, correspond to perpendicular domains, which are found in small droplets, and bottle-cap morphologies, which are observed in large droplets. The transition between these two morphologies occurs for droplet diameters in the vicinity of 200 nm.

correlation between droplet height, diameter, and morphology. For droplets with a diameter smaller than  $\approx 200$  nm (approximately  $5L_0$ ), height increases monotonically with diameter, and perpendicular domains form over the entire droplet. Above that diameter threshold, height remains constant at  $\approx 22$  nm, which corresponds to half of the lamellar periodicity,  $L_0/2$ . This could correspond to the formation of a parallel structure, comprising a single macromolecule layer, at

the center of the droplet. Going out of the droplet, as the height profile decreases, perpendicular domains could be forming around the edge. Figure 5 shows AFM height profiles of one

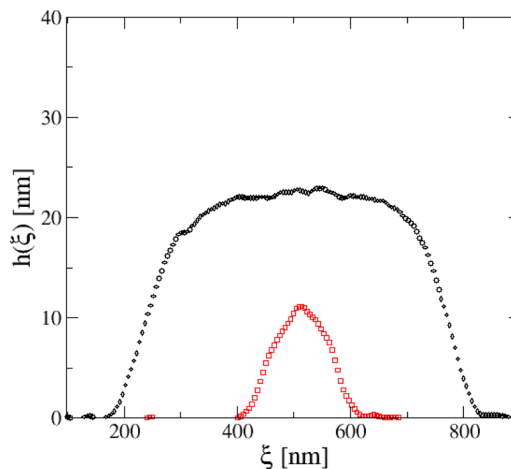


**Figure 5.** AFM droplet profiles for two different diameters from conditions in Figure 3. Note that the scale along  $x$ -axis is 10 $\times$  larger than that associated with the height.

small and one large BCP droplet. As can be seen in the figure, their shapes are different: the larger droplet is a flat disk, and the smaller droplet (with perpendicular ordering) is a spherical cap.

The experimental SEM images shown in Figures 1 and 3 only provide a top-down view of the droplets, and in the absence of a detailed model, the internal distribution of material can only be postulated. To fill this gap, the simulations described above are used to gain additional insights into the physical forces responsible for the observed morphological behavior. As shown in Figure 6, it is possible to control surface and interfacial

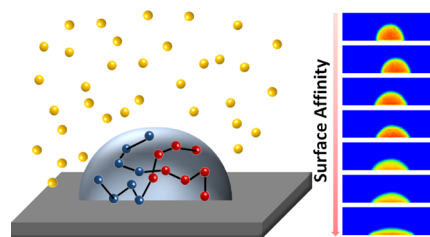


**Figure 6.** Schematic representation of simulation setup used to describe block copolymer droplets deposited on a substrate. By controlling surface affinity it is possible to control contact angle, as shown on the right image.

energies by tuning  $\lambda^u$  and  $\chi_{\mu\nu}$ , respectively. In particular, a large substrate surface energy can be represented by choosing a high value of  $\lambda^{A,B}$ . A first series of simulations were carried out to establish the effect of substrate surface energy on contact angle for a simple homopolymer droplet ( $\chi_{AB} = 0$ ), with polymerization index  $N = N_{AB}$ . The resulting two-dimensional density profiles are shown in the right panel of Figure 6; these profiles indicate that smaller contact angles can be achieved by increasing  $\lambda$ . We summarize these results in a quantitative manner by plotting the cosine of contact angle as a function of  $\Lambda = \lambda N$  in Figure 7.<sup>18</sup> All different wetting states can be realized, from partial to complete, by varying  $\Lambda$ . Note that a wetting transition occurs for  $\Lambda > 2.75$ . The statistical noise of

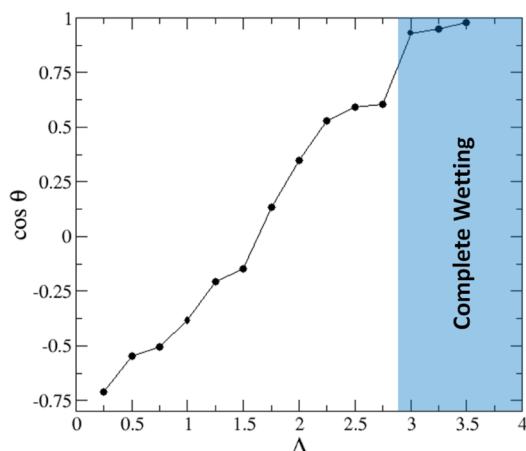


**Figure 7.** Contact angle of a homopolymer droplet ( $\chi = 0$ ) as a function of surface affinity  $\Lambda$ . A wetting transition occurs for  $\Lambda > 2.75$ .

our simulation results preclude us from identifying the character of such a transition (continuous or first order). Also note that by choosing proper values of  $\Lambda^{A,B}$  ( $= \lambda^{A,B} N_{AB}$ ), one can control the affinity of the substrate for one or the other block. Under nonpreferential conditions, i.e.  $\Lambda^A = \Lambda^B$ , regardless of contact angle, we always find perpendicular domains. However, for preferential substrates, the contact angle is important in defining the internal domain arrangement. Figure 8 shows two representative block copolymer droplet

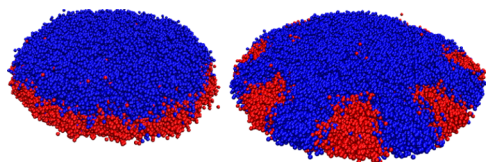


**Figure 8.** Representative configurations of block copolymer droplets for two different surface affinity values: one below the wetting transition  $\Lambda^A = \Lambda^B/0.85 = 2$  (left) and the other above the wetting transition  $\Lambda^A = \Lambda^B/0.85 = 3$  (right).<sup>43</sup>

configurations. Both have the same volume (number of polymers), on a preferential substrate, but the wetting conditions are different. In both cases, the preferential block is the dominant component wetting the substrate. In the first case, the preferential block corresponds to a condition where  $\Lambda < 2.75$  (large contact angle). In the second case  $\Lambda > 2.75$  (very small contact angle or complete wetting). For large contact angles, the morphology resembles a disk-like Janus particle. But, when the contact angle is small, parallel and perpendicular domains appear. These latter structures are the same as those observed in our experiments.

Our results above indicate that substrate surface energies are important factors governing the internal organization of block copolymer domains in nanoscale droplets and that good agreement with experiments for PS-preferential substrates is obtained when very small contact angles or complete wetting conditions are achieved. We therefore focus on those conditions and perform additional simulations to explore the effect of droplet size as well as that of the affinity of the substrate for one block. The latter is quantified by  $\Delta\Lambda = \Lambda^A - \Lambda^B$ . Our simulation results can be summarized as a morphology landscape in the  $(V_D, \Delta\Lambda)$  parameter space, shown in Figure 9, where  $V_D = n_{AB} N_{AB} / \rho_0$  is the volume of the

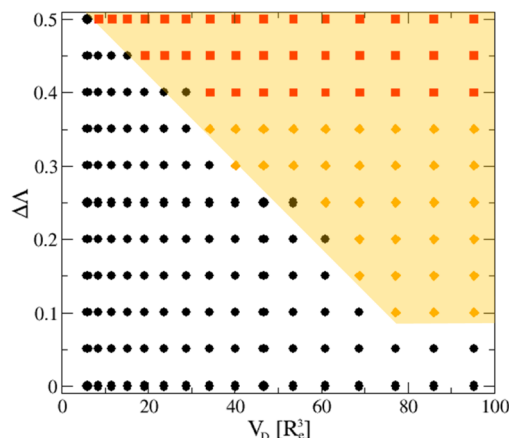


**Figure 9.** Diagram of morphologies obtained for different droplet sizes and  $\Delta\Lambda$ , the difference in surface affinity for one or the other block. Black dots correspond to perpendicular domains (P), orange diamonds are mixed morphologies (M), and red squares correspond to decorated disks (D).  $\Lambda^A = 3$ .

droplet (and is roughly proportional to its size). The resulting simulated morphologies can be classified into three groups: perpendicularly oriented domains (P), parallel layers decorated with perpendicular domains around the edges (bottle caps) (D), and mixed morphologies, where perpendicular domains contain a small parallel disk close to the center of the droplet (M).<sup>44</sup> These three groups are also observed in our experiments (see for example, the two close pairs of droplets enclosed by blue circles at the center of Figure 3 and the ones enclosed by red circles). On nonpreferential ( $\Delta\Lambda = 0$ ) or slightly preferential substrates, block copolymer droplets with perpendicularly oriented domains are always obtained, regardless of droplet size, as shown by the representative configurations of Figure 10. At intermediate  $\Delta\Lambda$ , a transition

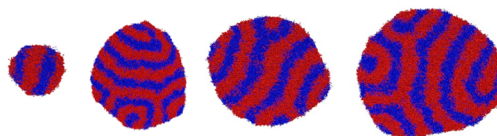


**Figure 10.** Top-view of representative droplet configurations on a nonpreferential substrate for different droplet sizes.  $\Delta\Lambda = 0.1$ .<sup>43</sup>

from P to M morphologies occurs as droplet size increases. By increasing  $\Delta\Lambda$ , the disk at the center of M morphologies increases in size and leads to D morphologies; in other words, we see a transition from P to D as droplet size increases. As can be seen in Figure 11, small droplets exhibit perpendicular domains, but beyond a critical droplet size, a transition to a D morphology occurs. Interestingly, the larger  $\Delta\Lambda$ , the smaller the critical droplet size. The D morphology exhibits the same general features as those seen in experiments, including the fact

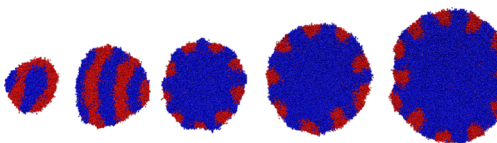


**Figure 11.** Top-view of representative droplet configurations on a PS-preferential conditions for different droplet sizes.  $\Delta\Lambda = 0.45$ .<sup>43</sup>

that droplet height reaches a value of  $L_0/2$  above this critical diameter. Our explanation of the structure of such “decorated” droplets is based on chain entropy. At high contact angle, chains can easily arrange into conformations where the end-to-end vector is oriented perpendicular to the substrate, as in a polymer brush. However, for small contact angle conditions, chains must either compress, to maintain the end-to-end vector oriented perpendicular to the substrate, or stretch, reorienting the end-to-end vector with a large parallel component along substrate. In both cases, such configurations would incur into a large configurational entropic penalty. The material avoids this scenario by reorganizing the molecules at the edge of the droplet with an end-to-end vector parallel to the substrate, even if that entails an enthalpic cost. Not surprisingly, such a reorganization also dictates a specific orientation for the perpendicular domains along the edge: locally, perpendicular and parallel lamellae grains minimize surface area by creating a Scherk-like interface,<sup>19</sup> with grains oriented perpendicular to each other, as seen in large droplets. It is also instructive to compare this peculiar behavior with that displayed when a BCP is confined into a film incommensurate with the bulk domain period. If the surfaces are slightly selective, then the equilibrium state adopted by the droplets corresponds to perpendicular domains. This orientation is driven by chain entropy, as above. When selectivity increases, then mixed or complex morphologies arise depending on whether symmetric or asymmetric boundary conditions are imposed.<sup>25</sup> In that sense, the centers of the decorated droplets find themselves in a frustrated, incommensurate condition, but the material at the droplet's edge is not, thereby leading to a perpendicular orientation. Note, however, that this condition (nonhomogeneous height profile) arises from the small contact angle constraint.

At this point it is also instructive to recall earlier experimental observations by Carvalho and Thomas,<sup>20</sup> who presented a study of terraces in block copolymer films deposited on preferential surfaces. On these substrates, block copolymers were found to adopt a parallel orientation. However, these authors also observed the “presence of reoriented lamellae at the boundary between terraces”. It was hypothesized that the reason for such perpendicular domains at terrace borders was due to the formation of a minimal surface. In particular, it was proposed that a Scherk surface spanning the whole film thickness was created, giving rise to the perpendicular features at the border. On the basis of our results above, we propose an alternative explanation for such an observation: terraces can be viewed as droplets deposited on a high surface energy film (the parallel lamellae). The low contact angle or wetting condition then induces the formation of perpendicular features at the terraces' edge. Clearly, if the surface energy between blocks is different, then this factor will play a role in defining the morphology. In our simulations, we have assumed that both blocks have the same surface energy. Experimentally, for PS and PMMA blocks the difference in surface energy is vanishing small at the temperatures at which our samples were annealed (see Model and Methods section). Also note that in order to achieve higher surface energies in our simulations, our model would require large values of the Flory–Huggins parameter, which can lead to numerical difficulties that are best addressed through other theoretical representations. Our simulations therefore only provide a general, qualitative description of copolymer droplets that is in agreement with experiments but one that should be revisited in the future with more detailed models.

Simulations could also be used to explore the influence of other parameters on droplet morphology. In particular, by increasing  $\chi_{AB}$ , it is expected that interfacial energy will play an important role in defining the global shape of the droplets. Indeed, the results of our Monte Carlo simulations for droplets deposited on nonpreferential substrates for different  $\chi_{AB}$ , shown in Figure 12, suggest that by increasing  $\chi_{AB}$  the droplets become

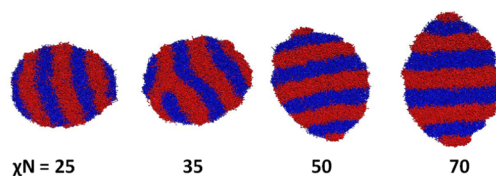


**Figure 12.** Top view of representative droplet configurations for different  $\chi$  values for same droplet size under nonpreferential conditions.<sup>43</sup>

more asymmetric. Specifically, they become elongated along the normal of the lamellar layers. Interestingly, anisotropic shapes have been observed experimentally when droplets are formed in solution, where surfactants are used to control polymer–solvent interfacial energies.<sup>27,29</sup> Also, these configurations have been observed in simulations using a lattice model of polymers.<sup>28</sup> Two possible explanations have been advanced in the past for the origins of the anisotropic droplet shape. One relies on the anisotropy of the interfacial tension between the block copolymer droplet and the surrounding medium.<sup>26,28</sup> However, Jang et al. performed SCFT calculations and found that such interfacial anisotropy is quite weak; they reported that a stronger contribution comes from incommensurability effects associated with the preferred lamellar spacing of the confined diblock and, therefore, with the interfacial energy associated with polymer domains.<sup>29</sup> Thus, in that view, the balance between surface and interfacial energies dictates again the internal domain organization and droplet shape.

## CONCLUSIONS

In this work, we have presented a systematic study of the structure of nanoscale block copolymer droplets. We have identified the role played by contact angle conditions on droplet shape and morphology. In contrast to available studies of directed copolymer self-assembly in thin films, where the surface energies of the substrate and the polymeric material (in the case of blocks with similar surface tension) are not relevant to the process, in droplets they are crucial in defining the equilibrium morphology. In particular, when a preferential substrate is used, a transition is observed with droplet size from a morphology with perpendicularly oriented domains to a morphology containing a central parallel layer decorated with perpendicular structures at the edge. Through the use of a molecular model, we have been able to interpret this transition in terms of the interplay of 3-D soft confinement, configurational chain entropy, and interfacial and surface energies.

Block copolymers are increasingly finding applications in lithography, where their characteristic period is used to reduce the feature sizes that can be created with standard lithographic tools. In such applications, the block copolymer material “adds” information to the process which is inherent in its ordered structure. In the same manner, the copolymer droplets discussed in this work could be used as the basis for development of inks that incorporate feature sizes that are

smaller than the dimensions of the droplets. The results presented in this work suggest that through a combination of synthesis and simulations it might be possible to design a new generation of structured inks for advanced printing applications.

## ■ ASSOCIATED CONTENT

### 📄 Supporting Information

Figures S1 and S2. The Supporting Information is available free of charge on the ACS Publications website at DOI: 10.1021/acs.macromol.5b00630.

## ■ AUTHOR INFORMATION

### Corresponding Authors

\*E-mail: jrogers@illinois.edu (J.A.R.).

\*E-mail: depablo@uchicago.edu (J.J.d.P.).

### Author Contributions

S.-M.H. and M.S.O. contributed equally to this work.

### Notes

The authors declare no competing financial interest.

## ■ ACKNOWLEDGMENTS

An award of computer time was provided by the INCITE program of the Argonne Leadership Computing Facility. We gratefully acknowledge the computing resources provided on Blues, high-performance computing cluster operated by the Laboratory Computing Resource Center at Argonne National Laboratory. S.M.H., A.R.H., P.F.N., and J.J.d.P. acknowledge support from U.S. Department of Energy, Office of Science, Basic Energy Sciences, Materials Science and Engineering Division. The experimental work was supported by the Air Force Office of Scientific Research MURI FA9550-12-1-0471.

## ■ REFERENCES

- (1) Rowlinson, J. S.; Widom, B. *Molecular Theory of Capillarity*; Dover: New York, 2002.
- (2) Bates, F. S.; Fredrickson, G. H. *Annu. Rev. Phys. Chem.* **1990**, *41*, 525.
- (3) Bates, F. S.; Fredrickson, G. H. *Phys. Today* **1999**, *52*, 32.
- (4) Hamley, I. W. *The Physics of Block Copolymers*; Oxford University Press: Oxford, 1998.
- (5) Liu, G.; Detcheverry, F. A.; Ramírez-Hernández, A.; Tada, Y.; Yoshida, H.; de Pablo, J. J.; Nealey, P. F. *Macromolecules* **2012**, *45*, 3986.
- (6) Liu, C. C.; Han, E.; Onses, M. S.; Thode, C. J.; et al. *Macromolecules* **2011**, *44*, 1876.
- (7) Onses, M. S.; Song, C.; Williamson, L.; et al. *Nat. Nanotechnol.* **2013**, *8*, 667.
- (8) Detcheverry, F. A.; Kang, H.; Daoulas, K. Ch.; Müller, M.; Nealey, P. F.; de Pablo, J. J. *Macromolecules* **2008**, *41*, 4989.
- (9) Fredrickson, G. H. *The Equilibrium Theory of Inhomogeneous Polymers*; Oxford University Press: Oxford, 2006.
- (10) Ruiz, R.; Kang, H.; Detcheverry, F. A.; Dobisz, E.; Kercher, D. S.; Albrecht, T. R.; de Pablo, J. J.; Nealey, P. F. *Science* **2008**, *321*, 936.
- (11) Kim, J. U.; Matsen, M. W. *Soft Matter* **2009**, *5*, 2889.
- (12) Stasiak, P.; McGraw, J. D.; Dalnoki-Veress, K.; Matsen, M. W. *Macromolecules* **2012**, *45*, 9531.
- (13) Hur, S. M.; García-Cervera, C. J.; Fredrickson, G. H. *Macromolecules* **2012**, *45*, 2905.
- (14) Helfand, E. *J. Chem. Phys.* **1975**, *62*, 999.
- (15) Q Pike, D.; Detcheverry, F. A.; Müller, M.; de Pablo, J. J. *J. Chem. Phys.* **2009**, *131*, 084903.
- (16) Ch.Daoulas, K.; Müller, M.; de Pablo, J. J.; Nealey, P. F.; Smith, G. D. *Soft Matter* **2006**, *2*, 573.
- (17) Frenkel, D.; Smit, B. *Understanding Molecular Simulations*, 2nd ed.; Academic Press: New York, 2002.

- (18) The calculation of contact angle was performed as implemented in: Milchev, A. I.; Milchev, A. A. *EPL* **2001**, *56*, 695 and Milchev, A. I.; Milchev, A. A.; Binder, K. *Comput. Phys. Commun.* **2002**, *146*, 38. Briefly, by using the cylindrical symmetry around the axis perpendicular to the substrate, we performed a spherical average of the density field  $\phi(r, \varphi, z)$ . Then, contours of constant density were computed and we defined the droplet–air interface as the contour with  $\phi^-(r, z) = 0.5$ . By fitting a tangent to this contour in the region close to the substrate, an estimate of the contact angle  $\theta$  was obtained.
- (19) Thomas, E. L.; et al. *Nature* **1988**, *334*, 598.
- (20) Carvalho, B. L.; Thomas, E. L. *Phys. Rev. Lett.* **1994**, *73*, 3321.
- (21) Petera, D.; Muthukumar, M. *J. Chem. Phys.* **1997**, *107*, 9640.
- (22) Tsori, Y.; Andelman, D. *Macromolecules* **2001**, *34*, 2719.
- (23) Wang, Q.; Nealey, P. F.; de Pablo, J. J. *Macromolecules* **2002**, *35*, 9563.
- (24) Ramírez-Hernández, A.; Suh, H. S.; Nealey, P. F.; de Pablo, J. J. *Macromolecules* **2014**, *47*, 3520.
- (25) Fasolka, M. J.; Mayes, A. M. *Annu. Rev. Mater. Res.* **2001**, *31*, 323.
- (26) Balsara, N. P.; Marques, C. M.; et al. *Phys. Rev. E* **2002**, *66*, 052802.
- (27) Jeon, S.-J.; Yi, G.-R.; Yang, S.-M. *Adv. Mater.* **2008**, *20*, 4103.
- (28) Chi, P.; Wang, Z.; Li, B.; Shi, A.-C. *Langmuir* **2011**, *27*, 11683.
- (29) Jang, S. G.; Audus, D. J.; Klinger, D.; et al. *J. Am. Chem. Soc.* **2013**, *135*, 6649.
- (30) Kondic, L.; Diez, J. A.; et al. *Phys. Rev. E* **2009**, *79*, 026302.
- (31) Diez, J. A.; et al. *Phys. Fluids* **2009**, *21*, 082105.
- (32) Fowlkes, J. D.; Kondic, L.; Diez, J. A.; et al. *Nanoscale* **2012**, *4*, 7376.
- (33) Green, P. F.; Limary, R. *Adv. Colloid Interface Sci.* **2001**, *94*, 53.
- (34) Limary, R.; Green, P. F.; Shull, K. R. *Eur. Phys. J. E* **2002**, *8*, 103.
- (35) Wu, S. J. *Phys. Chem.* **1970**, *74*, 632.
- (36) Ausserre, D.; Raghunathan, V.; Maaloum, M. *J. Phys. II* **1993**, *3*, 1485.
- (37) Croll, A. B.; Massa, M. V.; Matsen, M. W.; Dalnoki-Veress, K. *Phys. Rev. Lett.* **2006**, *97*, 204502.
- (38) Knoll, A.; Horvat, A.; Lyakhova, K. S.; et al. *Phys. Rev. Lett.* **2002**, *89*, 035501.
- (39) Farrell, R. A.; Kehagias, N.; Shaw, M. T.; et al. *ACS Nano* **2011**, *5*, 1073.
- (40) Mansky, P.; et al. *Phys. Rev. Lett.* **1997**, *79*, 237.
- (41) Han, E.; et al. *Macromolecules* **2009**, *42*, 4896.
- (42) Kim, S.; et al. *ACS Nano* **2013**, *11*, 9905.
- (43) Images created using VMD: Humphrey, W.; Dalke, A.; Schulten, K. *J. Mol. Graphics* **1996**, *14*, 33.
- (44) Notice that M and D morphologies only differ regarding the areal fraction of the parallel domain. Our distinction as two “different” morphologies highlights which “component” (parallel disk or perpendicular domains) dominates the global droplet internal organization. This helps to delimitate which parameters are better to be used in simulations to represent the experimental conditions, as we observed fewer M morphologies under the conditions studied.